Transparent Conductive Films Consisting of Ultralarge Graphene Sheets Produced by Langmuir–Blodgett Assembly

Qingbin Zheng, Wai Hing Ip, Xiuyi Lin, Nariman Yousefi, Kan Kan Yeung, Zhigang Li, and Jang-Kyo Kim*

Department of Mechanical Engineering, The Hong Kong University of Science and Technology, Clear Water Bay, Kowloon, Hong Kong

ABSTRACT Monolayer graphene oxide (GO) sheets with sizes ranging from a few to ~200 μm are synthesized based on a chemical method and are sorted out to obtain four different grades having uniform sizes. Transparent conductive films are produced using the ultralarge graphene oxide (UL-GO) sheets that are deposited layer-by-layer on a substrate using the Langmuir–Blodgett (LB) assembly technique. The density and degree of wrinkling of the UL-GO monolayers are turned from dilute, close-packed flat UL-GO to graphene oxide wrinkles (GOWs) and concentrated graphene oxide wrinkles (CGOWs) by varying the LB processing conditions. The method demonstrated here opens up a new avenue for high-yield fabrication of GOWs or CGOWs that are considered promising materials for hydrogen storage, supercapacitors, and nanomechanical devices. The films produced from UL-GO sheets with a close-packed flat structure exhibit exceptionally high electrical conductivity and transparency after thermal reduction and chemical doping treatments. A remarkable sheet resistance of ~500 Ω/sq at 90% transparency is obtained, which outperforms the graphene films grown on a Ni substrate by chemical vapor deposition. The technique used in this work to produce transparent conductive UL-GO thin films is facile, inexpensive, and tunable for mass production.

KEYWORDS: ultralarge graphene oxide · Langmuir–Blodgett assembly · transparent conductive films · graphene oxide wrinkles · self-assembly

Transparent conductors have been used in a wide variety of photoelectronic and photovoltaic devices, such as flat displays, solar cells, optical communication devices, and solid-state lighting.[1,2] Graphene, a two-dimensional monolayer of sp^2-bonded carbon atoms, has attracted significant interests recently because of the unique transport properties.[3] Due to the high optical transmittance and electrical conductivity, graphene is being considered as a transparent conductive electrode. Compared with traditional electrodes made from indium tin oxide or fluorine tin oxide, graphene films have high mechanical strength, flexibility, chemical stability, and are considered much cheaper to produce.

A key to success in such applications is to develop methods to produce large-size graphene sheets with high yields and deposit them onto a substrate uniformly in an aligned manner. The graphene sheets in current use for the fabrication of transparent conductors are relatively small, mostly with an area of hundreds of square micrometers.[4–8] The small area of graphene sheets results in high intersheet contact resistance due to a large amount of intersheet junctions.[9] To decrease the number of intersheet tunneling barriers, production of inherently large-size graphene sheets is highly desirable. Although mechanical cleavage of graphite was shown to prepare high-quality graphene with a millimeter size, the yield of this method is extremely low, being unsuitable for mass production.[10] Alternatively, graphitization of Si-terminated SiC (0001) in an argon atmosphere could produce monolayer graphene films with a domain size of several tens of micrometers.[11] However, the graphene obtained thereby was difficult to transfer to other substrates, and the yield was very low. The chemical vapor deposition (CVD) technique has been extensively explored to grow extremely large-area graphene on Ni films or Cu foils.[12–14] The CVD method usually requires specific substrate materials, which have to be removed chemically after the growth of graphene. The high cost of single crystal substrates and the ultrahigh vacuum conditions necessary to maintain the CVD growth significantly limit the use of the method for large-scale applications.[13]

Owing to the scalability of production and the convenience in processing, graphene oxide (GO) has been considered an important precursor for the fabrication of transparent conductors.[15] GO sheets are strongly hydrophilic and can produce stable and homogeneous colloidal suspensions in aqueous and various polar organic solvents due to the electrostatic repulsion between

* Address correspondence to mejkkim@ust.hk.

Received for review May 22, 2011 and accepted June 21, 2011.

Published online June 21, 2011
10.1021/nn2018683

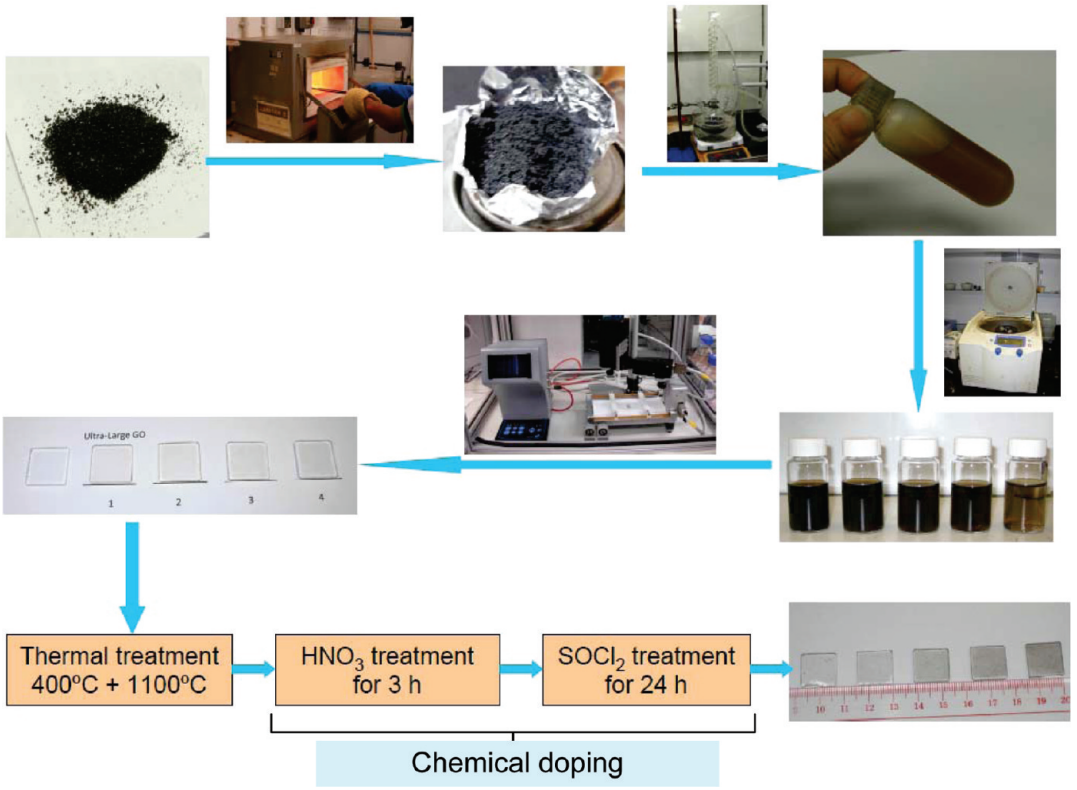

Figure 1. Flowchart for preparation of graphene thin films.

the negatively charged GO sheets. These GO dispersions are easy to process to produce transparent conductors on a substrate.[16] Transparent conductor films containing GO or chemically reduced GO sheets have been deposited *via* several well-established techniques, including spin- or spray-coating,[17,18] transfer printing,[5,19,20] dip-coating,[6] electrophoretic deposition,[21] and Langmuir–Blodgett (LB) assembly,[22,23] followed by chemical reduction and/or thermal annealing. Among these approaches, LB assembly is the only technique that can realize controllable deposition of GO in a layer-by-layer manner. The thickness of GO films can be accurately controlled upon repeated deposition, leading to optimized optical and electrical properties of the final products.[24]

In this report, we present an efficient and highly reproducible chemical method that involves pre-exfoliation of natural graphite flakes to produce gram quantities of ultralarge graphene oxide (UL-GO) sheets, up to ~50–200 μm in lateral size with a yield exceeding 50% by weight. The LB assembly technique is then used to transfer the GO monolayers onto substrates and produce highly conducting transparent LB thin films. After thermal reduction and chemical doping treatments, the transparent conductor made from the UL-GO sheets shows a sheet resistance of 459 Ω/sq at a transmittance of 90% along with a remarkable σ_{DC}/σ_{OP} ratio of 7.29. These values are better than those of the graphene films prepared by CVD on a Ni substrate, confirming the beneficial effects of both the ultralarge size of GO and layer-by-layer structure of the films.

RESULTS AND DISCUSSION

LB Assembly of GO. The process used to prepare monolayer UL-GO sheets is essentially similar to our previous reports[25,26] and is schematically illustrated in the flowchart in Figure 1. The sizes of the as-prepared GO sheets varied largely (Figure 2), making it difficult to control the occurrence of these morphological features. Therefore, before the LB deposition, the as-prepared GO dispersion was screened to separate the dispersions containing the smallest and the largest groups of GO sheets with uniform size distributions, namely, the small graphene oxide (S-GO) and UL-GO dispersions. S-GO and UL-GO dispersions were obtained through three runs of centrifugation and separation of the precipitate and supernatant of unsorted, as-prepared GO. The area of UL-GO sheets ranged from about 1 to 10 000 μm^2, while the area of S-GO sheets was several square micrometers on average. The surface pressure was monitored using a tensiometer during compression. The typical surface pressure–area isotherm shown in Figure 3a presents the change in the slope corresponding to the phase transition of GO sheets from gas to condensed liquid and to solid state. There existed an initial gas phase where the surface pressure remained essentially

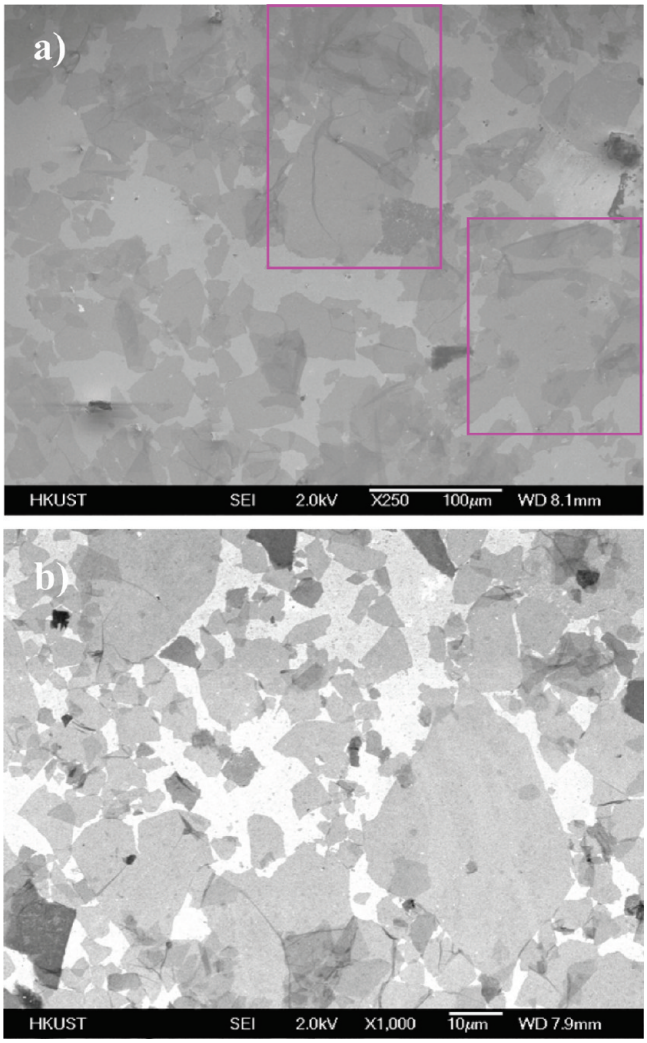

Figure 2. SEM images of as-prepared GO sheets deposited on a Si substrate at a constant surface pressure of 10 mN/m: (a) low magnification and (b) high magnification.

constant (stage a). The pressure began to increase as the compression continued (stage b) and the GO sheets were about to touch one another, tiling over the entire surface. The increase in surface pressure was likely due to the electrostatic repulsion between the GO sheets. Slight darkening of the monolayer color was observed, which is consistent with the increase in material density on the water surface. A further increase in surface pressure followed (stage c) when the monolayer was compressed beyond the close-packed stage. This occurred because the GO sheets started to fold at the touching points along their edges instead of overlapping on top of another. At a higher pressure (stage d), partial overlapping and wrinkling happened, leading to a nearly complete monolayer of interlocked GO.

The 2D GO monolayers thereby produced were stable and consistently showed the same quality as indicated by the fully reversible compression/expansion behavior of the GO sheets even after many cycles. Figure 3b shows the representative surface pressure curves plotted against area for two cycles of compression/expansion without sample collection, confirming that the curves had nearly the same shape and final pressure. It is worth noting that there is a small shift of the gas–liquid phase transition point toward a smaller area as the cycles continued, indicating the loss of a small amount of material from the monolayer after each cycle.[22]

The GO films produced on quartz substrates were reduced thermally to obtain reduced ultralarge graphene oxide (rUL-GO). To further improve the optical transparency and electrical characteristics of transparent conductors, a series of additional treatments were employed, as schematically illustrated in the flowchart in Figure 1. The final products are designated as the chemically doped, reduced ultralarge graphene oxide (C-rUL-GO) films.

Control of GO Structure. When the GO sheets were brought together side-by-side during the LB assembly, several unique microscopic morphologies were observed through the interactions between the neighboring GO sheets: namely, wrinkles, folds, and overlaps. These

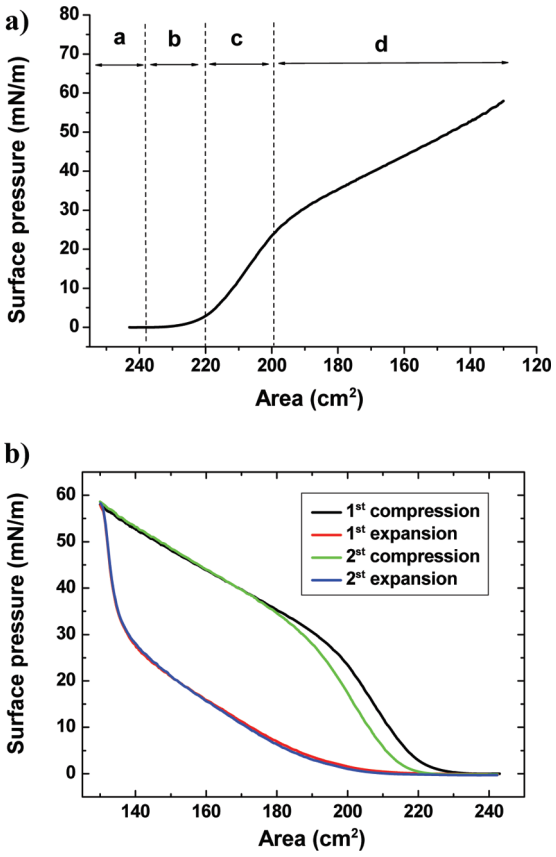

Figure 3. (a) Surface pressure *vs* area plot showing the corresponding four stages (a–d) of the formation of GO monolayers in LB assemly; (b) isotherm plots of two sequential compression/expansion cycles, confirming highly reversible and stable GO monolayer against compression. The two curves essentially overlap on top of another over the whole area, except at the early stage of compression.

morphological features are undesirable as they reduce the optical transparency of the GO films.[27] Figure 4 shows the SEM images of LB-assembled S-GO sheets collected on a silicon substrate at different stages of isothermal compression using the S-GO dispersion. As the surface compression increased, the packing density increased continuously from (a) isolated S-GO sheets to (b) close-packed S-GO sheets, (c) overpacked GO sheets with folded edges, and (d) overpacked S-GO sheets with folded edges and overlapping on top of another.[23] It is also worth noting that the rigid S-GO sheets collected from the LB assembly were free of wrinkles, while other methods, such as drop-casting, spin-coating, and spraying, usually produced wrinkled sheets.[4,5,28]

The corresponding SEM images for the UL-GO sheets are given in Figure 5. Due to the large size ranging from a few tens to ~200 μm, the UL-GO sheets tend to be softer and more flexible than S-GO sheets, presenting microscopic morphologies distinct from those observed in S-GO sheets depending on the pressure applied. Typical features include (a) isolated UL-GO sheets, (b) close-packed UL-GO sheets, (c) overlapped UL-GO sheets with some wrinkles, and (d) overlapped UL-GO sheets with extensive wrinkles, in the increasing order of the surface pressure or the packing density. It appears that at a high surface pressure the UL-GO sheets tended to wrinkle while the S-GO sheets were more prone to overlap. When the surface pressure was low (0 to ~10 mN/m), the films collected at this stage consisted of dilute, well isolated, flat individual UL-GO sheets (Figure 5a,b). With increasing surface compression beyond the close-packed region, the UL-GO sheets were forced to squeeze each other, leading to overlapping and buckling. Figure 5c,d shows typical graphene oxide wrinkles (GOWs) with different degrees of wrinkling. The hydrogen bonds present between the carboxylic acid edge groups encouraged the interactions between UL-GO edges and thus prevented them from sliding, which in turn contributed to wrinkling of UL-GO sheets. Because of the irregularly shaped polyhedrons with polydisperse sizes of UL-GO sheets, they would squeeze each other from random directions, resulting in wrinkling with random orientations. These wrinkles tended to be aligned along the contact lines of neighboring sheets, confirming the source of wrinkling being caused by buckling developed under in-plane compression.

In an effort to control the degree of wrinkling, different pulling speeds were used during the LB transfer. Figure 5e,f shows a much higher degree of wrinkling in the UL-GO films obtained at a higher pulling speed of 1.0 mm/min, designating it "concentrated graphene oxide wrinkles" (CGOWs). The LB transfer of flat GO sheets is a self-assembly process whose quality depends largely on the evaporation of water molecules present between UL-GO sheets and substrate. The relatively small size of S-GO allowed water to evaporate easily, and thus wrinkle-free S-GO films were obtained (Figure 4). However, the water droplets are often trapped between the UL-GO sheets, and the capillary force induced by water evaporation causes wrinkling of the sheets.[29,30] In particular, if a high pulling speed is applied, there would be too short a time for the UL-GO sheets to relax into a flat state and transfer onto the substrate. In this case, water may not be fully evaporated, causing wrinkling to occur during the transfer process due to the capillary force and gravity (Figure 5g). This may explain why the UL-GO sheets assembled at a high pulling speed of 1.0 mm/min and a high surface pressure of 30 mN/m became CGOWs after transfer. Other than the fast pulling speed, the compression of the films can also cause wrinkling even before deposition onto the substrate.

A novel approach has recently been reported for direct fabrication of graphene oxide nanoribbons with varying widths and lengths by plasma etching of GOWs.[31] Single- or double-layer graphene oxide nanoribbons were obtained through the accurate control of plasma etching conditions so that the top layers of

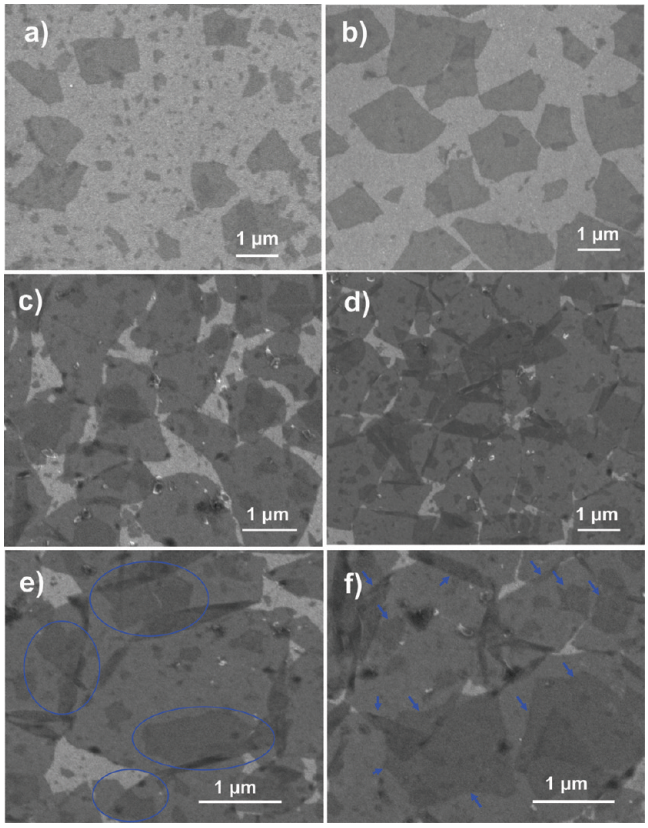

Figure 4. SEM images of S-GO sheets collected on a silicon substrate at different stages of surface pressure (see Figure 3a). The packaging density increases from (a) isolated S-GO sheets to (b) close-packed S-GO sheets, (c) overpacked S-GO sheets with folded edges, and overpacked S-GO sheets with overlapping, taken at a (d) low magnification and (e,f) high magnification.

GOWs acted as sacrificial layers. However, the GOWs used in the above study did not have enough wrinkles, and there is no established method to control the wrinkles on the surface of GO. The method proposed in this study offers a facile and environment-friendly approach to prepare large-size GOs with controllable amounts of wrinkles on their surface. Because GOWs and CGOWs have no caps at their ends, it may be easier to encapsulate functional molecules or nanomaterials in the internal cavities of GOs than in carbon nanotubes.[32,33] In addition, the interlayer distance of the wrinkles can also be tailored to better accommodate intercalants of various sizes.[34] The UL-GO sheets with high density wrinkles, such as GOWs and CGOWs, make them promising candidates for many applications, including hydrogen storage, supercapacitors, and nanomechanical devices. Table 1 summarizes various GO structures that can be obtained at different pulling speeds and surface pressures along with their potential applications.

Surface Morphology. GO could form a colloidal solution in water due to electrostatic repulsion between the ionized carboxylic and phenol hydroxyl groups that are located on the basal plane of GO sheets with a negative charge.[26] When the second GO layer was deposited on top of the first layer in our study, these two layers were likely to experience both electrostatic repulsion and van der Waals attraction. Since the GO sheets are brought together on top of another, their van der Waals potential can be scaled with $(1/d^2)$.[35] The residual π-conjugated domains can also contribute to the attraction between GO sheets. While these attractive forces dominate and lead to successful layer-by-layer deposition of GO sheets, the GO sheets also experience electrostatic repulsion from both their neighbors and those already deposited, causing wrinkling to occur. In particular, wrinkling becomes serious when depositing a large number of layers because the substrate is no longer flat due to the presence of GO sheets deposited previously.[22]

The typical surface morphologies of as prepared UL-GO and rUL-GO films after thermal treatment are shown in Figure 6, and the corresponding arithmetical mean roughness, root-mean-square roughness, and peak to peak roughness values are summarized in Figure 7a–c. The surface roughness of both films increased consistently with increasing number of GO layers. The parabolic increase, instead of a linear increase, may indicate that the wrinkles have been accumulated after each GO layer, deteriorating the flatness of the films. It is also worth noting that the surface roughness was consistently reduced after the thermal treatment due to the removal of oxygenated functional groups and graphitization of the films at an

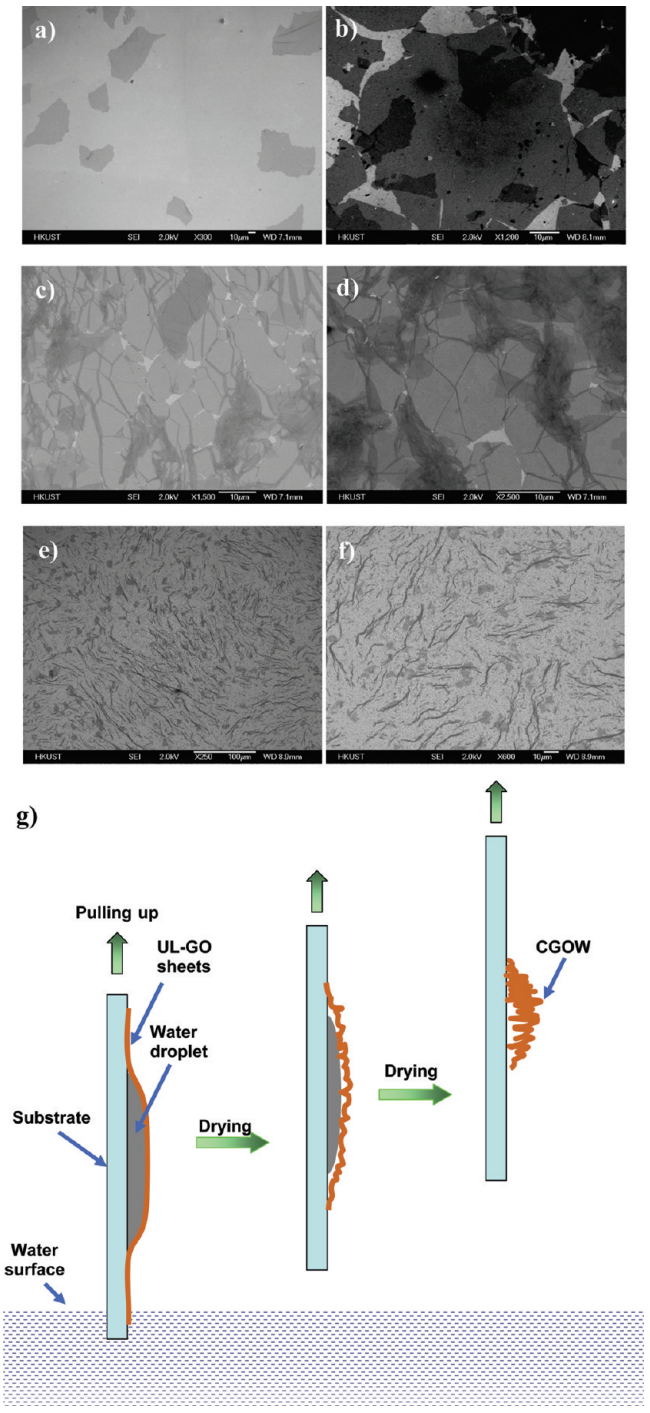

Figure 5. (a–d) SEM images of UL-GO sheets collected on a silicon wafer at different stages of surface pressure (see Figure 3a) at a pulling speed of 0.1 mm/min. The packaging density increases from (a) isolated UL-GO sheets to (b) close-packed UL-GO sheets, (c) overlapped UL-GO sheets with some wrinkles, and (d) overlapped UL-GO sheets with extensive wrinkles. (e,f) SEM images of UL-GO sheets collected on a silicon substrate at stage d of the surface pressure curve (see Figure 3a) at a pulling speed of 1.0 mm/min: concentrated GO wrinkles (CGOWs), taken at (e) low and (f) high magnifications. (g) Schematics for the generation of CGOWs due to capillary forces.

elevated temperature.[19,20] Although the wrinkles and defects cannot be completely removed after thermal treatment, due to the very well-aligned structure of the LB films, the surface roughness was much lower than the films produced by other techniques, such as spin- or spray-coating,[17,18] dip-coating,[6] and transfer printing.[5,19,20] The thickness of the deposited UL-GO films was measured using the AFM (Figure S4 in the Supporting Information) and is plotted in Figure 7d. It is interesting to note that the average thickness of the film made from one UL-GO layer was ~1.9 nm, which is about 50% higher than the literature value[36,37] and the AFM measurement in our study (Figure S1a). This observation is not surprising in light of the

TABLE 1. Various GO Structures Obtained at Different Pulling Speeds and Surface Pressures

type of GO	pulling speed (mm/min)	surface pressure (mN/m)	structure	applications
S-GO	0.1—1.0	any	flat GO	nanoelectronic devices
UL-GO	0.1	0—15	flat GO	micro- and nanoelectronic devices
UL-GO	0.1	>20	GOWs	fabrication of graphene oxide nanoribbons
UL-GO	1.0	>20	CGOWs	hydrogen storage, microcircuit interconnects

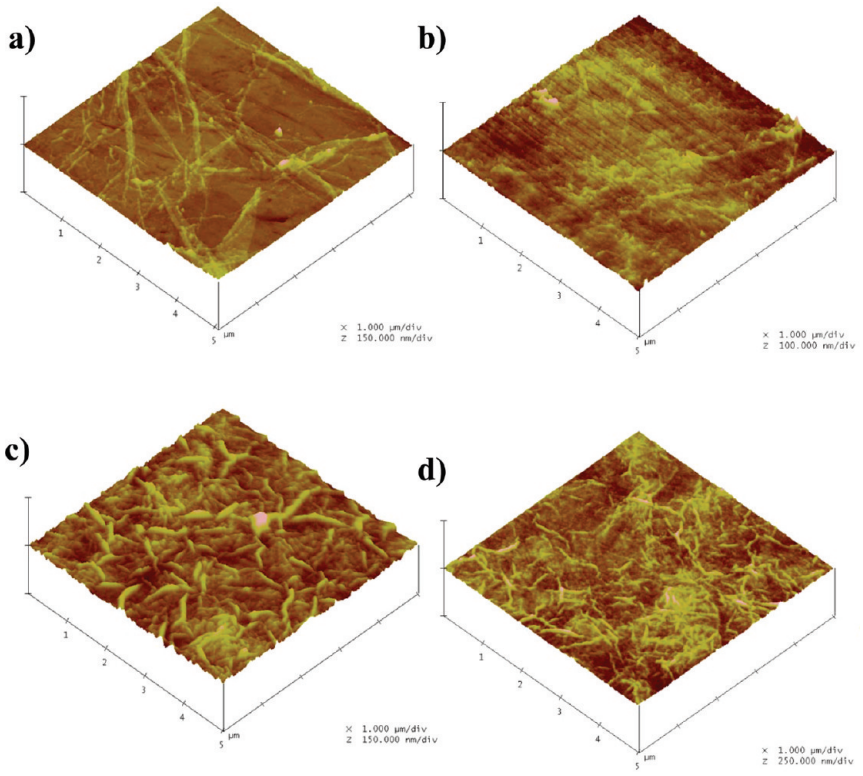

Figure 6. AFM images of GO films consisting of two layers (a,b) and eight layers (c,d) of monolayer GO sheets taken before (a,c) and after thermal treatment (b,d).

corresponding roughness of the film, which is about 1 nm (Figure 7a) due to wrinkling of UL-GO sheets.

Optical Transmittance and Electrical Conductivity. Comparison of optical and electrical properties between UL-GO films with different number of layers obtained at different stages of treatment is presented in Figure 8. A thicker film resulted in a higher degree of absorption of light and thus a lower transparency at all treatment stages studied. The transparency was significantly deteriorated after the thermal treatment, whereas part of the lost transparency was restored after the chemical treatments (Figure 8a,b).[20] The films darkened after the thermal treatment due to the reduction of GO and the adsorption of impurity particles on the other side of quartz substrates, which was an artifact. The removal of these impurities by the subsequent acid treatment contributed to the improvement of transparency. Due to the graphitization effect of the high-temperature annealing, there was a strong interaction between the rUL-GO and quartz substrate after thermal treatment. The films maintained good integrity after acid treatment, and no peeling was observed.

The sheet resistance values of the graphene films measured after the thermal treatment were in the range of 277—605 Ω/sq for films with thickness of 3.7—18.5 nm (Figure 8c), which is much lower than our previous finding on the graphene films obtained by transfer printing, 1598 Ω/sq for a 38.7 nm thick film.[20] The thermal treatment removed part of the oxygenated functional groups and helped graphitization of graphene films, which in turn restored the π-electron system in graphene. After the chemical treatments, the sheet resistance was reduced by about 30—50% to 197—459 Ω/sq depending on the film thickness.

The degradation of the electrical conductivity improved by various chemical processes is a critical issue for practical applications in service environment.[20,38] To evaluate whether these properties remain stable, the sheet resistance of the C-rUL-GO film was measured after 4 months of exposure to ambient air and

the results are presented in Figure 8c. It is shown that the sheet resistance increased by about 10−30% after exposure depending on the film thickness. A possible reason for the degradation of conductivity is the loss of chloride functional groups that have an ameliorating effect of enhancing the electrical conductivity. The acyl chloride groups are reactive with water, and thus it is likely that the doped functional groups on the graphene film surface may have reacted with moisture present in air during aging. To reduce the possibility of decomposition and thus to retain the improved electrical conductivity, it was proposed to apply a protective coating made from poly(3,4-ethylenedioxythiop-Hhene)/poly(styrenesulfonate) (PEDOT/PSS).[39]

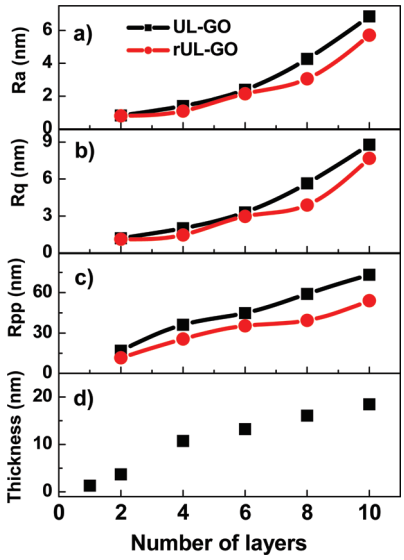

Figure 7. Film surface roughness of films in terms of (a) arithmetical mean, R_a, (b) root-mean-square, R_q, and (c) peak-to-peak roughness, R_{pp}. (d) Film thickness as a function of the number of layers.

Surface Chemistry. Raman spectra of natural graphite and UL-GO obtained before and after thermal treatment and chemical doping are shown in Figure 9a,c. Owing to the presence of isolated double bonds that resonate at frequencies higher than that of the G-band of graphite, the G-band peak of UL-GO was up-shifted from 1581 to 1607 cm^{-1}.[40,41] The corresponding G-band after the thermal reduction (rUL-GO) occurred at 1590 cm^{-1}, which represented the recovery of the hexagonal network of carbon atoms containing defects. Due to the possibility of charge transfer reaction between (host) carbon in graphene and (guest) chloride,[42] the G-band of C-rUL-GO (1587 cm^{-1}) was marginally down-shifted. The high electronegativity of

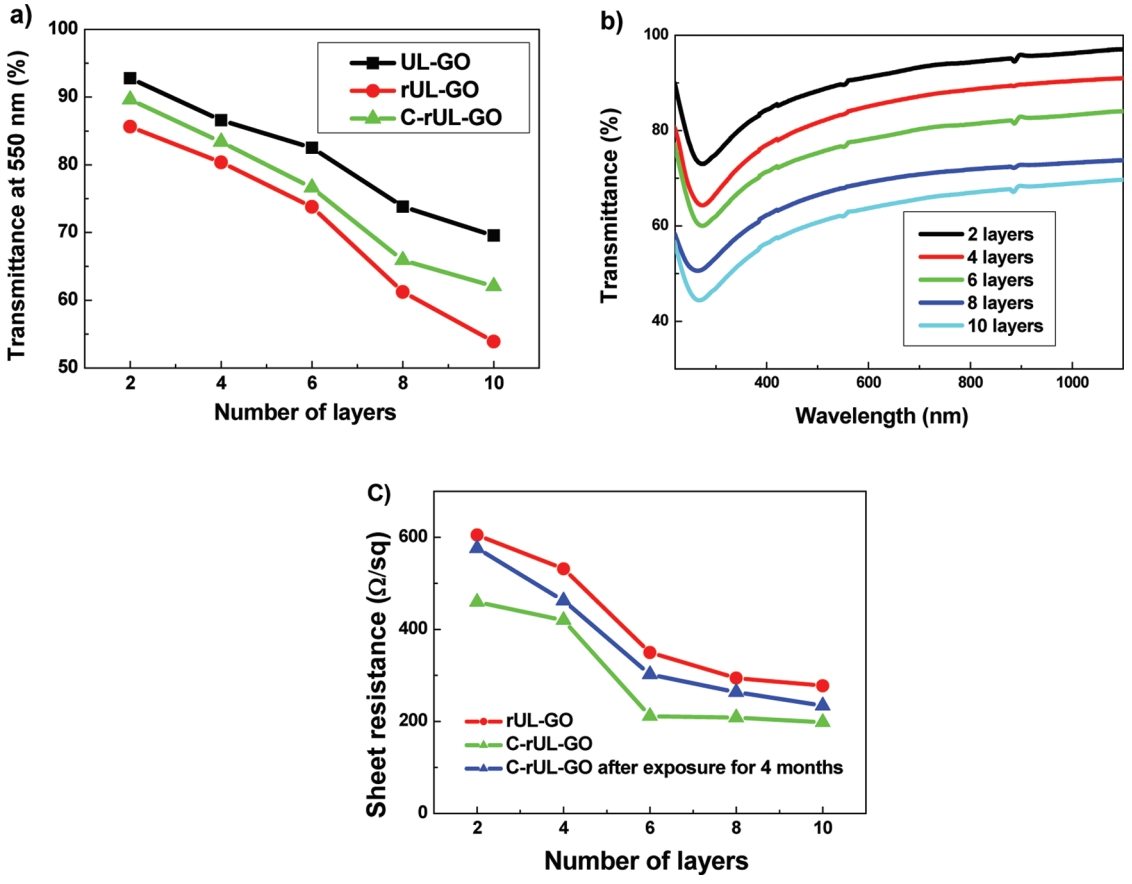

Figure 8. Comparison of optical and electrical properties between UL-GO films of different number of layers taken at different stages of treatment: (a) transmittance measured at 550 nm wavelength; (b) transmittance spectra of C-rUL-GO films as a function of wavelength; and (c) sheet resistance at different stages.

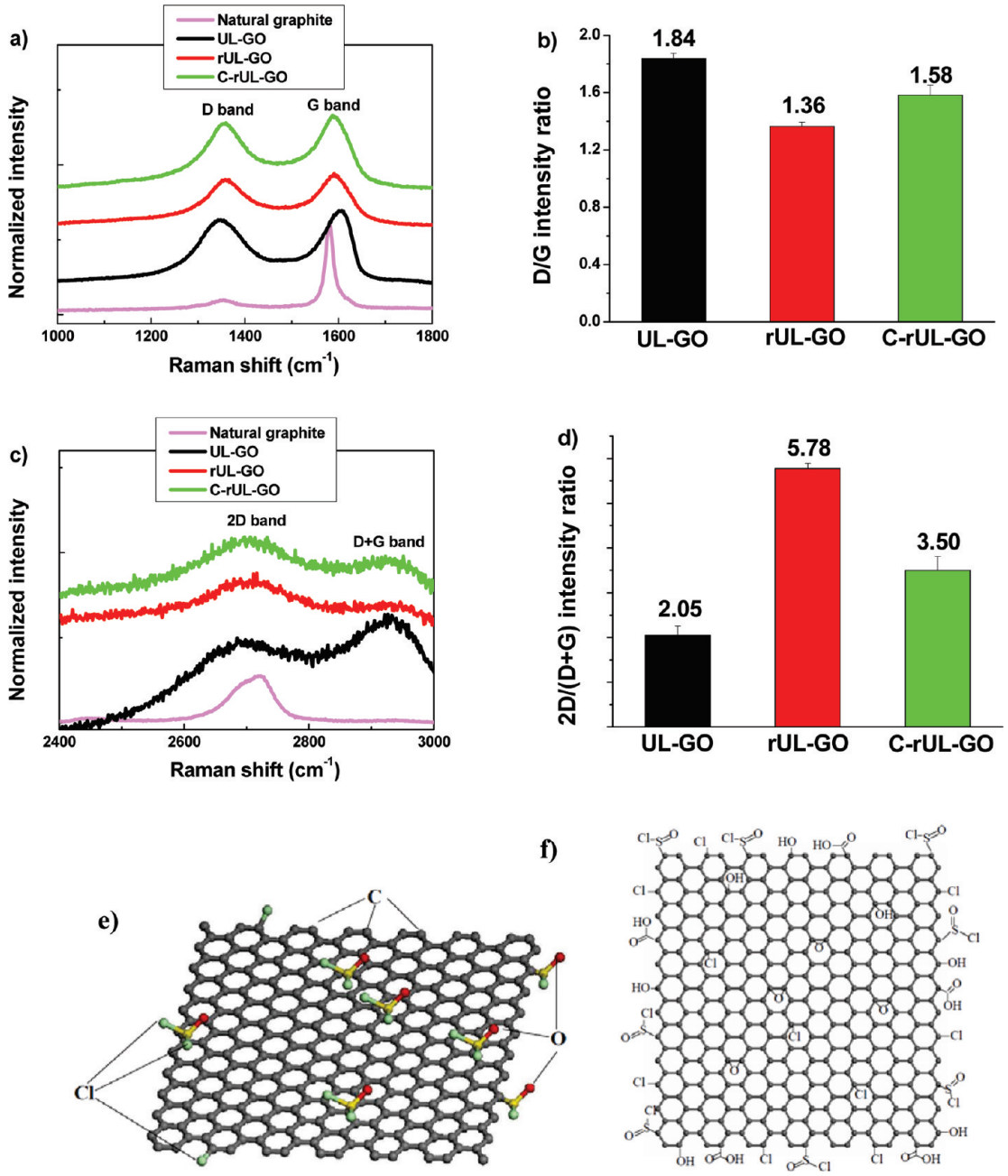

Figure 9. (a,c) Raman spectra for natural graphite, UL-GO, rUL-GO, and C-rUL-GO; and (b,d) the corresponding D/G and 2D/(D+G) intensity ratios. Schematic illustrations of (e) molecular structure of $SOCl_2$ molecules absorbed onto graphene surface; and (f) chemical structure of graphene sheet after chemical doping treatments.

chloride species encouraged carbon−chloride interactions that in turn triggered charge transfer reaction and created holes in graphene.

The G-band is Raman active for sp^2-hybridized carbon-based material, while the D-band is activated only if defects participate the double resonance Raman scattering near *K* point of Brillouin zone.[43] Hence, the intensity ratio of I_D/I_G is often used for estimating the sp^2 domain size of graphite-based materials. The I_D/I_G ratio of rUL-GO was indeed notably lower than UL-GO (Figure 9b), indicating that the thermal reduction process removed the functional groups and recovered the graphitic structure with less defects. However, the I_D/I_G ratio increased after the chemical treatments that again altered the graphene structure. Besides the G- and D-bands, there are two other Raman bands, called 2D and D+G at 2600−3000 cm^{-1} (Figure 9c), which are often ignored due to their weak intensities compared to D- and G-bands. The 2D-band is Raman-active for crystalline graphitic materials and is sensitive to the π-band in the graphitic electronic structure, while the combination mode of D+G is induced by disorder.[43] Here, we propose that it is very easy to distinguish the electronic conjugation of UL-GO obtained at different

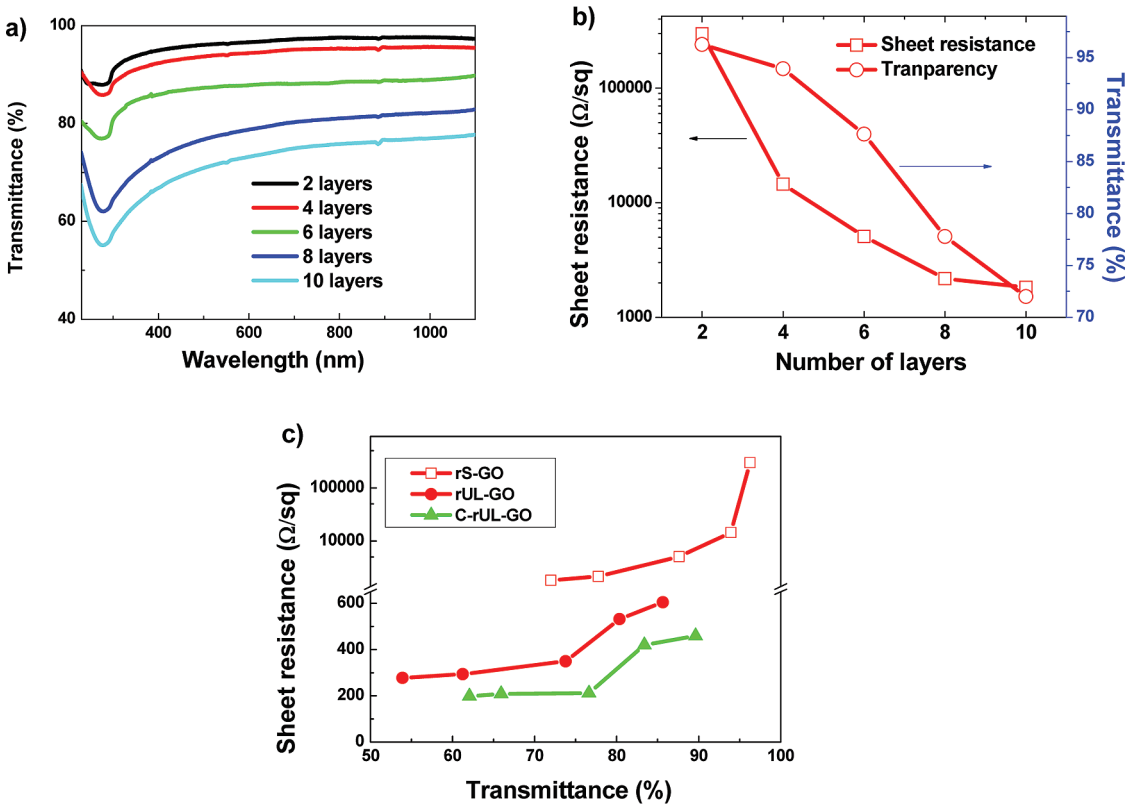

Figure 10. Optical and electrical properties of S-GO films made from different number of layers: (a) transmittance spectra as a function of wavelength; and (b) sheet resistance and transmittance of rS-GO LB films consisting of different number of layers; (c) sheet resistance and transmittance measured at 550 nm for transparent conductors consisting of rS-GO, rUL-GO, and C-rUL-GO.

stages of reduction and treatments by comparing these two bands. The intensity ratio I_{2D}/I_{D+G} shown in Figure 9d indicates that the I_{2D}/I_{D+G} ratio was more sensitive to the change in electronic conjugation from UL-GO to rUL-GO than the I_D/I_G ratio (Figure 9b), as a reflection of the recovery of graphitic electronic conjugation. The reduction of the I_{2D}/I_{D+G} ratio corresponding to the modification from rUL-GO to C-rUL-GO indicates that the newly doped functional groups, such as −Cl, −SOCl, and −COOH, introduced disorder again. Overall, the above discussion based on the Raman results is consistent with the XPS analysis in Supporting Information.

In summary, the combined effect of both HNO_3 cleaning and $SOCl_2$ doping resulted in enhanced electrical and optical properties. The effect of HNO_3 treatment is two-fold, namely, the removal of the impurities originated from thermal annealing and the etching of graphene film beneficial to electrical conductivity. $SOCl_2$ doping treatment introduced −Cl or −SOCl functional groups with a strong electronegativity onto the graphene surface and acting as electron acceptors to improve the electrical conductivity. Figure 9e,f presents schematic illustrations of the doping effect: $SOCl_2$ molecules are attached onto the graphene sheets, and −Cl or −SOCl functional groups are bonded after doping with $SOCl_2$. These molecules and functional groups with strong electronegativity acted as electron acceptors, allowing the Fermi level to move toward the valence band and thus increasing the hole density in graphene, giving rise to a significantly increased electrical conductivity.

Comparison with S-GO Films and Literature Data. Figure 10a,b presents the transmittance and sheet resistance of the films prepared from the S-GO sheets of typical lateral size of 1−3 μm, respectively. Compared to the films made from UL-GO sheets of typical size 50−200 μm, the transmittance of S-GO films showed marginally higher values over the whole film thicknesses and wavelengths studied, whereas its electrical resistance was significantly higher. The direct comparison between the films made from GO sheets of two different sizes using the same processing conditions in Figure 10c clearly indicates the benefits of using the large-size GO sheets. The rUL-GO sheets showed a much lower sheet resistance than the rS-GO sheets, by a remarkable 1 order of magnitude, for a given transmittance of the film. The decrease in the number of intersheet tunneling barriers in a continuous rGO film due to the increase in average size or sheet area of GO from several square micrometers to thousands of square micrometers was responsible for this observation.[44] The two-step chemical and doping treatments further reduced the resistivity by almost 50%.

The DC to optical conductivity ratio has been proposed to measure the figure of merit that can characterize the relative performance in terms of transparency and sheet conductivity between transparent conductors with different thicknesses and prepared using different synthesis routes and materials.[45] The relationship between transparency (T) and sheet resistance (R_s) is controlled by the conductivity ratio, σ_{DC}/σ_{OP}, using the equation

$$\frac{\sigma_{DC}}{\sigma_{OP}} = \frac{Z_0}{2R_s(T^{-1/2} - 1)} \quad (1)$$

where $Z_0 = 377\ \Omega$ is the impedance of free space. A high σ_{DC}/σ_{OP} ratio represents a high transmittance and a low sheet resistance, and thus high opto-electrical properties of transparent conductors, and *vice versa*. Table S3 in Supporting Information lists the calculated σ_{DC}/σ_{OP} values for transparent conductors made by different methods, including LB deposition, CVD, transfer printing, spin-, spray-, or dip-coating.[44] The σ_{DC}/σ_{OP} ratio of the transparent conductors made from UL-GO sheets in this study was 7.29 for C-rUL-GO consisting of two graphene layers, which outperformed the transparent conductors made by LB deposition, transfer printing, spin-, spray-, or dip-coating. Assuming relatively small-size graphene or GO sheets used previously, the above positive revelation confirms that the electrical conductivity of graphene films is limited mainly by intersheet junctions.[3] More surprisingly, our σ_{DC}/σ_{OP} ratio is even higher than that of graphene films prepared by CVD on a Ni substrate (σ_{DC}/σ_{OP} of *ca.* 2−6; see Table S3), demonstrating great potential for fabricating high-performance transparent conductors using UL-GO sheets and highly efficient two-step chemical and doping treatments. In addition, the CVD method usually requires certain substrate materials to be used, and the high cost of these single crystal substrate materials significantly limits the use of CVD method for large-scale applications.[13] As described above, films derived from aqueous suspensions of UL-GO through the LB method can avoid these limitations.

CONCLUSIONS

Transparent conductive films made from graphene or GO sheets have been considered as potential replacements for indium tin oxide transparent conductors. Developing methods to produce large-size GO sheets with high yield and promote their electrical conductivities is the key to success in such electronic applications. We demonstrate here that UL-GO sheets of ∼50−200 μm in lateral size can be obtained by a combination of thermal expansion and modified chemical methods. The LB assembly technique is used to transfer the GO monolayers onto a substrate layer-by-layer. By varying the surface pressure and pulling speed during the LB assembly, the film density and the formation of wrinkling can be tailored to produce different topological features, namely, dilute, close-packed flat UL-GO, GOWs, and CGOWs. The UL-GO sheets containing high density wrinkles, such as GOWs and CGOWs, produced in this study make them ideal candidates for applications in hydrogen storage, supercapacitors, and nanomechanical devices.

The electrical conductivities of transparent conductors made from closed-packed flat UL-GO and S-GO sheets are improved by a combination of thermal reduction and chemical doping treatments. The transparent conductors made from UL-GO sheets show a sheet resistance of 459 Ω/sq at a transmittance of 90% along with a remarkable σ_{DC}/σ_{OP} ratio of 7.29. The comparison with literature data clearly indicates that the transparent conductors produced in this study outperform the transparent conductors made by LB deposition and other methods, such as transfer printing, spin-, spray-, or dip-coating methods. Most notably, the opto-electrical properties of our product are even better than those of the graphene films prepared by CVD on a Ni substrate.

METHODS

Preparation of UL-GO. Five grams of natural graphite flakes (Asbury Graphite Mills) and 150 mL of sulfuric acid (H_2SO_4, General Chemical) were mixed and stirred in a round-bottom flask at a speed of 200 rpm. Fifty milliliters of fuming nitric acid was added into the mixture. The mixture was kept at room temperature and stirred for 24 h. Two-hundred milliliters of deionized water was then poured slowly into the mixture. The resultant mixture was washed using DI water, followed by centrifugation and drying at 60 °C for 24 h to obtain graphite intercalation compound. The dry graphite intercalation compound powder was thermally expanded at 1050 °C for 15 s to obtain expanded graphite that was used for the production of GO. One gram of expanded graphite and 200 mL of sulfuric acid were mixed and stirred in a three-neck flask. Ten grams of $KMnO_4$ was added to the mixture while stirring. The solution was transferred into an ice bath, and 200 mL of deionized water and 50 mL of H_2O_2 were poured slowly into the mixture, realizing color change of the suspension to light brown. The GO particles were washed and centrifuged with a HCl solution three times, then centrifuged again and washed with deionized water until the pH of the solution became about 5 to 6. The GO particles obtained thereby were diluted using DI water (∼1 mg/mL) and dispersed by gentle shaking.

Grading of Polydisperse GO Sheets. The as-prepared GO sheets with polydispersity in size need to be grouped into a few different size grades for efficient use. Four groups of GO sheets were obtained through three runs of centrifugation of unsorted, as-prepared GO. The GO solution was initially centrifuged at 8000 rpm for 40 min on a table-top centrifuge (SIGMA 2-16P), producing supernatant and precipitate. The precipitate was collected for the second run of centrifugation, while the supernatant was labeled as S-GO. The collected precipitate was dispersed in water again and centrifuged at 6000 rpm for 25 min, again producing supernatant and precipitate (large GO).

The precipitate was dispersed in water again for the third run of centrifugation at 4000 rpm for 25 min, producing supernatant (very large GO) and precipitate (UL-GO). Both the UL-GO and S-GO sheets were used in this study for the assembly of LB thin films.

Preparation of LB Films. Because the GO monolayers are very sensitive to surface-active impurities, all parts of the LB trough had to be thoroughly cleaned before each experiment. In addition, to minimize any contamination, plastic ware or rubber should not be used during storage and handling of the solvent and dispersion. If the hydrophilic GO monolayers were applied directly onto the deionized water surface, most GO submerged without spreading onto the water surface. To allow spreading of GO monolayers, a volatile solvent has to be mixed with water. Common water-immiscible solvents, such as chloroform or toluene, are not suitable for this purpose. Meanwhile, GO monolayers tended to collapse and adopt 3D compact conformations in nonpolar solvents such as acetone.[46] Therefore, methanol—a polar alcohol—was chosen as the solvent, which was proven to spread GO rapidly onto the water surface.[22]

A DI water/methanol mixture in the ratio of 1:5 was filled into the LB trough (KSV Instruments Ltd., MiniMicro L-B System), and the GO dispersion was slowly spread onto the water surface dropwise using a glass syringe. The solution was applied at a speed of 100 μL/min up to a total of 5 mL, and the GO monolayer formed thereby was stabilized for about 20 min before compression. The GO monolayer was compressed by moving barriers at a speed of 10 mm/min, while the surface pressure was monitored using a tensiometer attached to a Wilhelmy plate. At the end of the compression, a GO film with faint brown color could be observed. The GO monolayer was transferred to a substrate at various stages of compression based on a dip-coating method: a quartz substrate was vertically dipped into the trough and pulled out at a speed of 0.1 mm/min, and transfer of GO film occurred when the meniscus was spread on the substrate during pulling out. The effect of pulling speed was also studied for UL-GO. The substrate surface had to be maintained hydrophilic for proper wetting by water and efficient deposition of GO film. Poor deposition was observed on a hydrophobic surface that was obtained after a silane treatment of silicon or glass.[22] Typically, wafers made from silicon, glass, quartz, and mica were cleaned for about 30 min before deposition using a Piranha solution consisting of a sulfuric acid and peroxide in the ratio of $V_{H_2SO_4}/V_{H_2O_2}$ = 7:3.

To produce transparent conductors with uniform coverage and low optical scattering loss, multilayer GO films were transferred onto the substrate by sequential, layer-by-layer deposition of close-packed GO monolayers. Wrinkles, folds, and overlaps had to be avoided as they have strong light scattering effects.[27] Upon deposition of each GO monolayer, the substrate was either dried in air overnight or baked in an oven at 80 °C for 1 h to stabilize the adhesion of GO layer to the substrate. The deposition of the next GO layer was repeated to produce transparent conductor films consisting of 2 to 10 GO monolayers.

Reduction and Doping of GO Thin Films. The substrates were loaded inside a ceramic container with open ends, which was introduced into a furnace (Thermcraft/Eurotherm) with controlled vacuum and gas flow. A vacuum of 10^{-5} Torr was established before heating. The films were heated with a continuous flow of ultrapure argon, at a rate of 10 °C/min, held at 400 °C for 1.5 h at 10^{-3} Torr, and were allowed to cool to room temperature for about 20 min. Subsequently, the films were heated to 1100 °C at a rate of 10 °C/min and were held at the same temperature for 0.5 h. After cooling to room temperature, ambient air was admitted to the furnace and the films were recovered to obtain rUL-GO. The choice of 1100 °C as the graphitization temperature was confirmed effective previously,[19,20] and the flow of argon gas would eliminate the problem of film loss by reaction with residual oxygen. The rUL-GO obtained after the thermal treatment was subject to additional chemical doping treatments to obtain C-rUL-GO: namely, (i) dipping in a HNO_3 bath for 3 h and drying with gentle nitrogen flow; and (ii) dipping in a $SOCl_2$ bath for 24 h and drying with gentle nitrogen flow.

Characterization. Scanning electron microscope (SEM, JSM-6700F, JEOL) and field emission transmission electron microscopy (TEM, 2010F, JEOL) were used to characterize the structure and morphology of GO. The tapping-mode atomic force microscope (AFM, Scanning Probe Microscope-NanoScope, Digital Instruments) was employed to evaluate the surface morphology and the thickness of GO films. The transparency was measured using the UV/vis spectroscopy (Perkin-Elmer Lambda 20). The sheet resistance of the films was measured using the four-point probe method (Scientific Equipment & Services). To reduce the contact resistance between the probes and the film surface, the four contact points were coated with silver paste. The elemental compositions and the assignments of the carbon peaks were characterized using the X-ray photoelectron spectroscopy (XPS, PHI5600 Physical Electronics), which was equipped with a monochromatic Al Kα X-ray source operated in a residual vacuum of 5×10^{-9} Torr. The high-resolution spectra were deconvoluted using a multitak software (Physical Electronics). Raman spectroscopy (Renishaw MicroRaman/Photoluminescence System) was used to analyze the effects of thermal reduction and chemical doping on crystal quality of graphene films.

Acknowledgment. This project was financially supported by Henkel International (ICIPLC001.07/08) and the Hong Kong Research Grant Council (614010). Q.B.Z. is partly supported by the Postgraduate Scholarship through the NanoTechnology Program of the School of Engineering at HKUST. Technical assistance from the Materials Characterization and Preparation Facilities (MCPF) of HKUST is appreciated.

Supporting Information Available: Characterization of GO, XPS analysis, AFM images used to measure the thickness of UL-GO films, and the calculated σ_{DC}/σ_{OP} values for transparent conductors made from different methods, including LB deposition, CVD-grown graphene, transfer printing, spin-coating, spray-coating, and dip-coating. This material is available free of charge *via* the Internet at http://pubs.acs.org.

REFERENCES AND NOTES

1. Wu, Z. C.; Chen, Z. H.; Du, X.; Logan, J. M.; Sippel, J.; Nikolou, M.; Kamaras, K.; Reynolds, J. R.; Tanner, D. B.; Hebard, A. F.; *et al.* Transparent, Conductive Carbon Nanotube Films. *Science* **2004**, *305*, 1273–1276.
2. Wang, X.; Zhi, L. J.; Tsao, N.; Tomovic, Z.; Li, J. L.; Mullen, K. Transparent Carbon Films as Electrodes in Organic Solar Cells. *Angew. Chem., Int. Ed.* **2008**, *47*, 2990–2992.
3. Geim, A. K.; Novoselov, K. S. The Rise of Graphene. *Nat. Mater.* **2007**, *6*, 183–191.
4. Becerril, H. A.; Mao, J.; Liu, Z.; Stoltenberg, R. M.; Bao, Z.; Chen, Y. Evaluation of Solution-Processed Reduced Graphene Oxide Films as Transparent Conductors. *ACS Nano* **2008**, *2*, 463–470.
5. Eda, G.; Fanchini, G.; Chhowalla, M. Large-Area Ultrathin Films of Reduced Graphene Oxide as a Transparent and Flexible Electronic Material. *Nat. Nanotechnol.* **2008**, *3*, 270–274.
6. Wang, X.; Zhi, L. J.; Mullen, K. Transparent, Conductive Graphene Electrodes for Dyesensitized Solar Cells. *Nano Lett.* **2008**, *8*, 323–327.
7. Zhu, Y.; Cai, W.; Piner, R. D.; Velamakanni, A.; Ruoff, R. S. Transparent Self-Assembled Films of Reduced Graphene Oxide Platelets. *Appl. Phys. Lett.* **2009**, *95*, 103104.
8. Kim, Y. K.; Min, D. H. Durable Large-Area Thin Films of Graphene/Carbon Nanotube Double Layers as a Transparent Electrode. *Langmuir* **2009**, *25*, 11302–11306.
9. Eda, G.; Lin, Y. Y.; Mattevi, C.; Yamaguchi, H.; Chen, H. A.; Chen, I. S.; Chen, C. W.; Chhowalla, M. Blue Photoluminescence from Chemically Derived Graphene Oxide. *Adv. Mater.* **2010**, *22*, 505–509.
10. Meyer, J. C.; Geim, A. K.; Katsnelson, M. I.; Novoselov, K. S.; Booth, T. J.; Roth, S. The Structure of Suspended Graphene Sheets. *Nature* **2007**, *446*, 60–63.
11. Emtsev, K. V.; Bostwick, A.; Horn, K.; Jobst, J.; Kellogg, G. L.; Ley, L.; McChesney, J. L.; Ohta, T.; Reshanov, S. A.; Rohrl, J.;

et al. Towards Wafer-Size Graphene Layers by Atmospheric Pressure Graphitization of Silicon Carbide. *Nat. Mater.* **2009**, *8*, 203–207.
12. Kim, K. S.; Zhao, Y.; Jang, H.; Lee, S. Y.; Kim, J. M.; Kim, K. S.; Ahn, J. H.; Kim, P.; Choi, J. Y.; Hong, B. H. Large-Scale Pattern Growth of Graphene Films for Stretchable Transparent Electrodes. *Nature* **2009**, *457*, 706–710.
13. Reina, A.; Jia, X.; Ho, J.; Nezich, D.; Son, H.; Bulovic, V.; Dresselhaus, M. S.; Kong, J. Large Area, Few-Layer Graphene Films on Arbitrary Substrates by Chemical Vapor Deposition. *Nano Lett.* **2009**, *9*, 30–35.
14. Bae, S.; Kim, H.; Lee, Y.; Xu, X.; Park, J. S.; Zheng, Y.; Balakrishnan, J.; Lei, T.; Kim, H. R.; Song, Y.; Kim, Y.-J.; *et al.* Roll-to-Roll Production of 30-in. Graphene Films for Transparent Electrodes. *Nat. Nanotechnol.* **2010**, *5*, 574–578.
15. Zhu, Y.; Murali, S.; Cai, W.; Li, X.; Suk, J. W.; Potts, J. R.; Ruoff, R. S. Graphene and Graphene Oxide: Synthesis, Properties, and Applications. *Adv. Mater.* **2010**, *22*, 3906–3924.
16. Dreyer, D. R.; Park, S.; Bielawski, C. W.; Ruoff, R. S. The Chemistry of Graphene Oxide. *Chem. Soc. Rev.* **2010**, *39*, 228–240.
17. Watcharotone, S.; Dikin, D. A.; Stankovich, S.; Piner, R.; Jung, I.; Dommett, G. H. B.; Evmenenko, G.; Wu, S. E.; Chen, S. F.; Liu, C. P.; *et al.* Graphene-Silica Composite Thin Films as Transparent Conductors. *Nano Lett.* **2007**, *7*, 1888–1892.
18. Blake, P.; Brimicombe, P. D.; Nair, R. R.; Booth, T. J.; Jiang, D.; Schedin, F.; Ponomarenko, L. A.; Morozov, S. V.; Gleeson, H. F.; Hill, E. W.; *et al.* Graphene-Based Liquid Crystal Device. *Nano Lett.* **2008**, *8*, 1704–1708.
19. Wang, S. J.; Geng, Y.; Zheng, Q. B.; Kim, J. K. Fabrication of Highly Conducting and Transparent Graphene Films. *Carbon* **2010**, *48*, 1815–1823.
20. Zheng, Q. B.; Gudarzi, M. M.; Wang, S. J.; Geng, Y.; Li, Z. G.; Kim, J. K. Improved Electrical and Optical Characteristics of Transparent Graphene Thin Films by Acid and Doping Treatments. *Carbon* **2011**, *49*, 2905–2916.
21. Lee, V.; Whittaker, L.; Jaye, C.; Baroudi, K. M.; Fischer, D. A.; Banerjee, S. Large-Area Chemically Modified Graphene Films: Electrophoretic Deposition and Characterization by Soft X-ray Absorption Spectroscopy. *Chem. Mater.* **2009**, *21*, 3905–3916.
22. Cote, L. J.; Kim, F.; Huang, J. X. Langmuir−Blodgett Assembly of Graphite Oxide Single Layers. *J. Am. Chem. Soc.* **2009**, *131*, 1043–1049.
23. Kim, F.; Cote, L. J.; Huang, J. X. Graphene Oxide: Surface Activity and Two-Dimensional Assembly. *Adv. Mater.* **2010**, *22*, 1954–1958.
24. Wassei, J. K.; Kaner, R. B. Graphene, a Promising Transparent Conductor. *Mater. Today* **2010**, *13*, 52–59.
25. Geng, Y.; Wang, S. J.; Kim, J. K. Preparation of Graphite Nanoplatelets and Graphene Sheets. *J. Colloid Interface Sci.* **2009**, *336*, 592–598.
26. Aboutalebi, S. H.; Gudarzi, M. M.; Zheng Q. B.; Kim, J. K. Spontaneous Formation of Liquid Crystal in Ultra Large Graphene Oxide Dispersions. *Adv. Funct. Mater.* **2011**, DOI: 10.1002/adfm.201100448.
27. Cote, L. J.; Kim, J.; Zhang, Z.; Sun, C.; Huang, J. X. Tunable Assembly of Graphene Oxide Surfactant Sheets: Wrinkles, Overlaps and Impacts on Thin Film Properties. *Soft Matter* **2010**, *6*, 6096–6101.
28. Gilje, S.; Han, S.; Wang, M.; Wang, K. L.; Kaner, R. B. A Chemical Route to Graphene for Device Applications. *Nano Lett.* **2007**, *7*, 3394–3398.
29. Kim, J.; Kim, F.; Huang, J. X. Seeing Graphene-Based Sheets. *Mater. Today* **2010**, *13*, 28–38.
30. Kim, J.; Cote, L. J.; Kim, F.; Huang, J. X. Visualizing Graphene Based Sheets by Fluorescence Quenching Microscopy. *J. Am. Chem. Soc.* **2010**, *132*, 260–267.
31. Zhou, X.; Lu, G.; Qi, X.; Wu, S.; Li, H.; Boey, F.; Zhang, H. A Method for Fabrication of Graphene Oxide Nanoribbons from Graphene Oxide Wrinkles. *J. Phys. Chem. C* **2009**, *113*, 19119–19122.
32. Cao, L.; Chen, H. Z.; Li, H. Y.; Zhou, H. B.; Sun, J. Z.; Zhang, X. B.; Wang, M. Fabrication of Rare-Earth Biphthalocyanine Encapsulated by Carbon Nanotubes Using a Capillary Filling Method. *Chem. Mater.* **2003**, *15*, 3247–3249.
33. Gao, X. P.; Zhang, Y.; Chen, X.; Pan, G. L.; Yan, J.; Wu, F.; Yuana, H. T.; Songa, D. Y. Carbon Nanotubes Filled with Metallic Nanowires. *Carbon* **2004**, *42*, 47–52.
34. Gao, Y.; Chen, X.; Xu, H.; Zou, Y.; Gu, R.; Xu, M.; Jen, A. K. Y.; Chen, H. Highly-Efficient Fabrication of Nanoscrolls from Functionalized Graphene Oxide by Langmuir−Blodgett Method. *Carbon* **2010**, *48*, 4475–4482.
35. Israelachvili, J. N. *Intermolecular and Surface Forces*, 2nd ed.; Academic Press: San Diego, CA, 1992; p 450.
36. Jung, I.; Vaupel, M.; Pelton, M.; Piner, R.; Dikin, D. A.; Stankovich, S.; An, J.; Ruoff, R. S. Characterization of Thermally Reduced Graphene Oxide by Imaging Ellipsometry. *J. Phys. Chem. C* **2008**, *112*, 8499–8506.
37. Li, X. L.; Zhang, G. Y.; Bai, X. D.; Sun, X. M.; Wang, X. R.; Wang, E. G.; Dai, H. J. Highly Conducting Graphene Sheets and Langmuir−Blodgett Films. *Nat. Nanotechnol.* **2008**, *3*, 538–542.
38. Kasry, A.; Kuroda, M. A.; Martyna, G. J.; Tulevski, G. S.; Bol, A. A. Chemical Doping of Large-Area Stacked Graphene Films for Use as Transparent, Conducting Electrodes. *ACS Nano* **2010**, *4*, 3839–3844.
39. Jackson, R.; Domercq, B.; Jain, R.; Kippelen, B.; Graham, S. Stability of Doped Transparent Carbon Nanotube Electrodes. *Adv. Funct. Mater.* **2008**, *18*, 2548–2554.
40. Voggu, R.; Das, B.; Routt, C. S.; Rao, C. N. Effects of Charge Transfer Interaction of Graphene with Electron Donor and Acceptor Molecules Examined Using Raman Spectroscopy and Cognate Techniques. *J. Phys.: Condens. Matter* **2008**, *20*, 472204.
41. Ferrari, A. C.; Robertson, J. Interpretation of Raman Spectra of Disordered and Amorphous Carbon. *Phys. Rev. B* **2000**, *61*, 14095–14107.
42. Barpanda, P.; Fanchini, G.; Amatucci, G. G. Structure, Surface Morphology and Electrochemical Properties of Brominated Activated Carbons. *Carbon* **2011**, *49*, 2538–2548.
43. Pimenta, M. A; Dresselhaus, G.; Dresselhaus, M. S.; Cancado, L. G.; Jorio, A.; Saito, R. Studying Disorder in Graphite-Based Systems by Raman Spectroscopy. *Phys. Chem. Chem. Phys.* **2007**, *9*, 1276–1291.
44. Zhao, J.; Pei, S.; Ren, W.; Gao, L.; Cheng, H. M. Efficient Preparation of Large-Area Graphene Oxide Sheets for Transparent Conductive Films. *ACS Nano* **2010**, *4*, 5245–5252.
45. De, S.; Coleman, J. N. Are There Fundamental Limitations on the Sheet Resistance and Transmittance of Thin Graphene Films? *ACS Nano* **2010**, *4*, 2713–2720.
46. Wen, X.; Garland, C. W.; Hwa, T.; Kardar, M.; Kokufuta, E.; Li, Y.; Orkisz, M.; Tanaka, T. Crumpled and Collapsed Conformation in Graphite Oxide Membranes. *Nature* **1992**, *355*, 426–428.